Surface & Coatings Technology 299 (2016) 65–70

Contents lists available at ScienceDirect

Surface & Coatings Technology

journal homepage: www.elsevier.com/locate/surfcoat

Comparison of the structural and corrosion properties of the graphene/$SiN_{(200)}$ coating system deposited on titanium alloy surfaces covered with SiN transition layers

M. Kalisz [a,*], M. Grobelny [a], M. Świniarskib [b], P. Firek [c]

[a] Motor Transport Institute, Centre for Material Testing, 80 Jagiellonska St, Warsaw, Poland
[b] Faculty of Physics, Warsaw University of Technology, 75 Koszykowa St, Warsaw, Poland
[c] Faculty of Electronics and Information Technology, Warsaw University of Technology, 75 Koszykowa St, Warsaw, Poland

ARTICLE INFO

Article history:
Received 24 February 2016
Revised 25 April 2016
Accepted in revised form 27 April 2016
Available online 28 April 2016

Keywords:
Silicon nitride thin film
Nanoindentation
Electrochemical properties
Graphene
Graphene hybrid system

ABSTRACT

In this paper, comparative studies of the structural and corrosion properties of SiN/graphene/SiN coating systems with various SiN transition layer thickness have been investigated. The coating systems were formed on Ti6Al4V alloy surfaces. The SiN transition layer thicknesses varied from 100 nm to 300 nm. The thickness of the upper silicon nitride thin film, in all examined cases, was 200 nm. The silicon nitride thin film was deposited using the Plasma Enhanced Chemical Vapour Deposition method. A graphene monolayer was transferred onto the silicon nitride surface using the "PMMA-mediated" method.

The structural characteristics of coating systems obtained were examined using Raman spectroscopy, optical profilometry and SEM measurements. The corrosion properties of the coating systems were determined by an analysis of the voltammetric curves.

The SiN/graphene/SiN coating system with a 300 nm thick silicon nitride transition layer is characterised by the best structural and corrosion properties of all tested coating systems. In this case, the surface of the top silicon nitride thin film has no holes or flakes, as opposed to the coating systems with 100 nm and 200 nm thick transition layers, in which the upper SiN thin film flaked and dropped off. The value of corrosion current density obtained for this sample was almost two orders of magnitude lower than the current density obtained for the other tested coating systems.

1. Introduction

Titanium alloys have many potential industrial applications, mainly owing to their good mechanical and corrosion properties and biocompatibility [1–3]. However, some of these applications are limited because of certain unsatisfactory surface parameters, i.e. low hardness, low wear resistance and low corrosion resistance in hot, concentrated and low - pH solutions [4–7]. To bypass these obstacles, many various surface treatment techniques are used. These methods include, burnishing and surface micro-shot peening and thermo-chemical treatment, in particular based on the PVD and CVD methods [8–11]. Another way to protect titanium alloys and improve their surface properties is the application of ceramic coatings, i.e. silicon nitride. Silicon nitride thin films can be described as materials with high density, low wear rates, good insulating properties, excellent Na^+ resistance, relatively high fracture toughness, strength, high temperature corrosion resistance in an oxidizing atmosphere and in a sulphidizing-oxidizing atmosphere [12] and excellent biocompatibility [13–15]. They are an excellent diffusion barrier against water and aggressive contaminants that can corrode titanium alloys [16]. Silicon nitride films can be deposited by low-pressure-chemical-vapour-deposition (LPCVD), plasma enhanced chemical vapour deposition (PECVD) and reactive radio frequency (r.f.) sputtering techniques, but their structural, mechanical and corrosion properties highly depend on the technological process used [17–19].

Graphene has already proven to be an alternative way to improve the surface properties of titanium alloys, especially corrosion resistance. Recent studies have shown that a single graphene layer considerably increases the corrosion resistance of materials such as copper [20], nickel [21] and titanium alloy [22] and protects the surface of those metals from oxidation [22]. Unfortunately, a single layer of graphene does not change the mechanical properties of the surface on which it is deposited [22].

Previous research has shown that a combination of two types of coatings, such as silicon nitride and graphene monolayer, in a hybrid coating system, having a thickness of several hundred nanometres, is

* Corresponding author.
E-mail address: malgorzata.kalisz@its.waw.pl (M. Kalisz).

http://dx.doi.org/10.1016/j.surfcoat.2016.04.064
0257-8972/

characterised by good mechanical properties and excellent corrosion resistance in aggressive environments, e.g. body fluids [23,24].

Unfortunately, this hybrid coating system also has a few disadvantages. As shown in recent studies, the graphene monolayer introduced at the structure interface, between the titanium alloy substrate and the silicon nitride coating system in graphene/SiN coating systems, reduces the adhesion of the silicon nitride thin film to the titanium substrate. The silicon nitride thin film breaks and comes away from the surface during the process of creating the hybrid system [23], significantly reducing its corrosion resistance.

The purpose of this manuscript is to show the effect of the silicon nitride transition layer, incorporated between the titanium alloy surface and the graphene/$SiN_{(200)}$ coating system on the structural and corrosion properties of the whole coating system. In this work, the structural and corrosion properties of the graphene/silicon $nitride_{(200)}$ coating system deposited on titanium alloy surfaces covered by the silicon nitride transition layer with three different thickness, has been investigated and compared with the pure titanium alloy and Ti-Al-V/SiN systems.

2. Materials and methods

2.1. Experimental design

2.1.1. Specimen preparation

For the purpose of the experiment, five sets of titanium alloy Ti6Al4V (ASTM Grade 5, UNS R56400) (Table 1) were prepared in the same manner. Before the technological processes, the Ti alloy surfaces were polished using Stuers RotoPol 21 grinding and polishing apparatus. The sample surface was polished to a "mirror finish". In the next stage, samples were cleaned in an acetone solution.

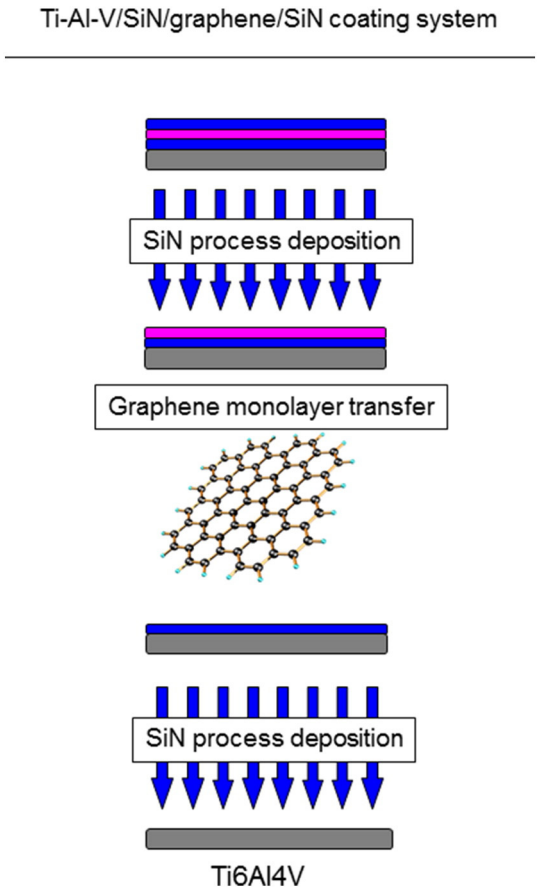

Fig. 1. Schematics showing the preparation of the test samples.

2.1.2. Preparation of the silicon nitride thin films

The amorphous silicon nitrides thin films were fabricated using the Oxford Plasma Technology PlasmaLab 80 Plus System, which is a parallel plate PECVD (13.56 MHz) deposition system. The system makes it possible to predefine the process parameter values and control them in real-time during the process. The films prepared using the PECVD method have a lot of advantages, such as low deposition temperature, high growth rate, good uniformity and good adhesion to the substrate surface [25].

2.1.3. Graphene monolayer preparation

The graphene monolayers were grown on 18-μm thick copper foil using the chemical vapour deposition (CVD) technique. For this purpose a home-made CVD set – based on a Blue M Tube Furnace with a 1-in. diameter reactor tube – was used. During the growth process the reactor chamber is set to a low pressure (~10^{-6} Torr) and heated up to ~1000 °C in hydrogen atmosphere. Methane is used as a carbon source (growth time is typically 10 min).

Graphene was transferred to the titanium alloy surfaces and the silicon nitride surfaces using the "PMMA-mediated" method [26]. First, the PMMA (495 K, about 100 nm thick) was spin-coated on top of the synthesised graphene on a copper substrate and dried for 24 h at room temperature. Next the graphene from the bottom of the Cu substrate was etched using a reactive ion etching method in oxygen plasma (PlasmaLab 80 +, Oxford Instruments). After that, the exposed Cu foil was dissolved in an aqueous etchant of iron (III) nitrate for several hours. When the copper dissolved the graphene sample was cleaned in DI (deionized) water. Next, the ion particles were removed using a hydrochloric acid solution, hydrogen peroxide as a catalyst dissolved in water [26]. After all the cleaning steps the PMMA/graphene layer was transferred to the examined surfaces and annealed in order to evaporate the water and increase the adhesion between the graphene and the surface. In the last step the PMMA layer was removed.

2.1.4. Preparation of test samples

In the Fig. 1 the schematic procedures for the preparation of the test samples are shown.

One set of 500 nm thick silicon nitride film and three sets of silicon nitride transition layers with different thickness (100 nm, 200 nm and 300 nm) were prepared. In the case of samples with silicon nitride transition layers, their surface was covered with a graphene monolayer. At the end, these same samples were covered with 200 nm thick silicon nitride thin films. In this way, four different coatings systems were prepared. These coatings systems were labelled: $SiN_{(500)}$, $SiN_{(100)}$/graphene/$SiN_{(200)}$, $SiN_{(200)}$/graphene/$SiN_{(200)}$ and $SiN_{(300)}$/graphene/$SiN_{(200)}$.

The sample covered with a 500 nm thick silicon nitride thin film was prepared in two processes with a pause to expose the sample to the atmosphere, similar to the sample covered with the $SiN_{(300)}$/graphene/$SiN_{(200)}$ coating system. The aim of this procedure was to minimalize the effect of the preparation of the samples on their structural and corrosion properties.

During the preparation of the silicon nitride thin films, the SiH_4 and NH_3 flow rates, r.f. power, temperature as well as the pressure in the chamber, were kept constant at 150 ml/min, 50 ml/min, 120 W, 350 °C and 0.8 Torr, respectively. The thickness of the deposited layers was controlled by the time of the deposition process, which varied from 1 min to 3 min.

Table 1
Composition of Ti6Al4V titanium alloy.

Components, wt.%						
C	Fe	N	O	Al	V	Ti
0.08	0.25	0.05	0.20	5.50–6.75	3.5–4.5	Bal

Table 2
Summary of the Si_xN_y process parameters.

d_{SiN} [nm]	100	200	300
RF Power [W]	120		
Pressure[Torr]	0.8		
SiH_4 gas flow [ml/min]	150		
NH_3 gas flow [ml/min]	50		
Temperature [°C]	350		
Time [min]	10	20	30

Table 2 shows a summary of the parameters used for the deposition of the SiN thin films in this study.

2.2. Analysis of surface characteristics

The quality and number of the transferred layers of graphene were evaluated by Raman spectroscopy (InVia Renishaw Spectrometer, 514 nm laser line, standard mode). All Raman spectra were collected at room temperature using 1 mW of laser power (on the sample).

Raman spectroscopy is a fast, non-destructive method for the study of e.g. various carbon materials. In the case of graphene, the Raman spectra give information about the number of layers [27–30], material quality and defects [27–30]. Typical Raman spectra consist of three main modes: D mode (~1350 cm^{-1}), G mode (~1580 cm^{-1}) and 2D mode (~2700 cm^{-1}). A monolayer graphene sheet is easily identified by a Raman study simply by looking at the G/2D relative intensity ratio (usually about 0.2), also taking into account the shape of the peaks [27–30]. The quality and defectiveness of the graphene sheet can be verified by the appearance of the D mode peak, usually taken as the relative I_D/I_G ratio [27–30].

The thickness of the deposited silicon nitride thin films was measured using a Taylor Hobson Talysurf CCI Lite optical profilometer. The measurements were performed after each silicon nitride thin film deposition process. The obtained results are show in Table 2.

The elemental composition and surface morphology of the deposited coating systems were investigated with the aid of a Zeiss FE-SEM Merlin with EDS Quantax System (Bruker) and Raith e-Line Plus (FE Zeiss column, 30 keV) scanning electron microscope.

The Raman spectroscopy measurements and SEM measurements and were performed after each step of the technological process, during the preparation of the test samples.

2.3. Electrochemical measurements

The electrochemical measurements were carried out in 0.5 M/l NaCl, 2g/l KF, pH = 2 adjusted by concentrated hydrochloric acid. The solution (0.5 M NaCl, pH 2 2 g/l KF) in which the electrochemical measurements were conducted is characterised by high corrosivity compared to titanium alloys. It is a more aggressive environment than that of typical electrolytes for corrosion tests (e.g. artificial saliva, SBF). Voltammetric measurements (polarization curves) were carried out at a scan rate of 1 mV/s within a range of −150 mV to 1000 mV versus open circuit potentials, and polarization curves corresponding to all examined materials were recorded. Prior to each polarization experiment, the samples were immersed in the electrolyte for 1 h while monitoring open circuit potential to establish steady state conditions. Each electrochemical measurement for the same material was performed three times. In the paper we show only the most representative results. However, the differences between the successive values of the open circuit potential (for the same material) did not exceed 50 mV. A three-electrode cell arrangement was applied using an Ag/AgCl electrode with a Luggin capillary as a reference electrode and a platinum wire as the auxiliary electrode (counter electrode). The measurements were carried out by means of an Autolab EcoChemie System of the AUTOLAB PGSTAT 302N type equipped with GPESv. 4.9. software in aerated solutions at room temperature. The values of the corrosion current densities (i_{corr}) were obtained from the polarization curves by the extrapolation of the cathodic and anodic branch of the polarization curves to the corrosion potential [31].

3. Results and discussion

3.1. Structural characterisation of the TiAlV/SiN/graphene/SiN/graphene coating systems

In Fig. 2 an exemplary SEM image is shown of a titanium alloy surface covered by silicon nitride thin films, corresponding to all measured samples. The surfaces of all measured samples are smooth, without cracks or damage.

In Fig. 3 an exemplary SEM image is shown of the graphene monolayer deposited on a silicon nitride transitions layer. This image is appropriate for each of the prepared samples. The sample surfaces remain smooth, without cracks or damage and with visible grains of the graphene layer.

In the Raman spectra for the graphene layers deposited on the respective silicon nitride transition layers, the negligible D mode is seen, suggesting that the graphene layer in each prepared sample is without structural defects. Furthermore the intensity ratio of the G and 2D modes shows that the deposited graphene layer, on each investigated sample, is indeed a graphene monolayer. In Fig. 4 an example Raman spectrum is shown, appropriate for each of the prepared samples.

In Fig. 5 SEM images are shown of silicon nitride thin films deposited on top of prepared coating structures. As the obtained results show, the structural properties of the deposited silicon nitride thin film depend on the thickness of the SiN transition layer.

For the $SiN_{(100)}$/graphene/$SiN_{(200)}$ and $SiN_{(200)}$/graphene/$SiN_{(200)}$ samples we found some areas where the SiN layer peeled away from the graphene surface forming holes in the upper SiN layer. The results obtained suggest low silicon nitride adhesion to the thin carbon layer. However, depending on the thickness of the silicon nitride transition layer, the size of the holes formed in the layer changes. The thicker the transition layer, the less damage to the upper SiN layer is observed (compare Fig. 5a and 5b).

For the $SiN_{(300)}$/graphene/$SiN_{(200)}$ coating system, in the surface of upper silicon nitride thin film, no cracks, deformation or defects were observed. The surface of the top silicon nitride thin film is without holes or flakes (see Fig. 5c).

For comparison, in Fig. 6 the SEM image of the silicon nitride thin film deposited on the titanium alloy surface covered a graphene monolayer, without a transition layer, is shown. In this image we found many areas where the SiN layer peeled away from the graphene surface

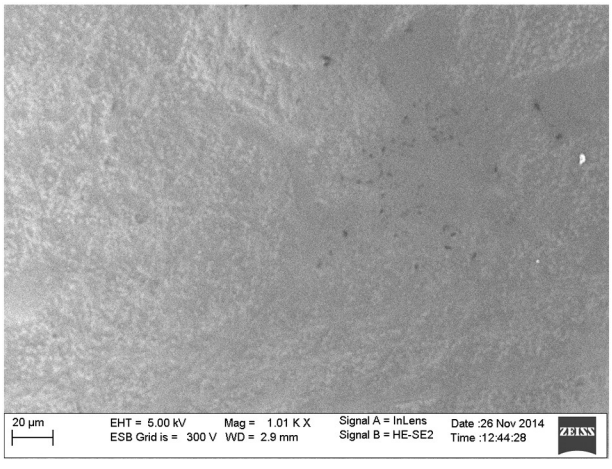

Fig. 2. An exemplary SEM image – deposited silicon nitride thin film.

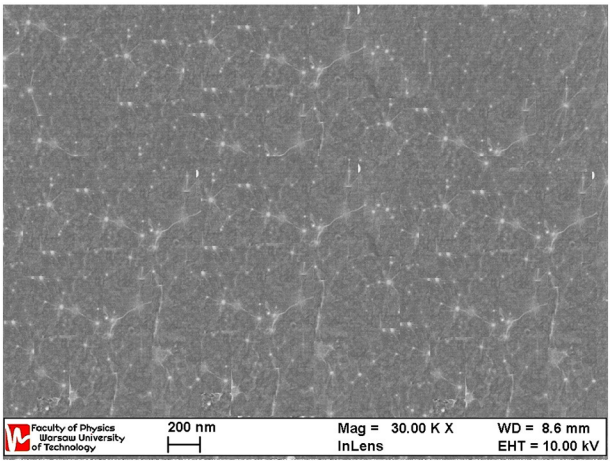

Fig. 3. An exemplary SEM image of a graphene monolayer deposited on a silicon nitride transition layer.

forming holes in the SiN layer, which suggests low silicon nitride adhesion to the thin carbon layer [23,24].

The Raman spectra collected in peeled off areas, in samples of $SiN_{(100)}$/graphene/$SiN_{(200)}$ and $SiN_{(200)}$/graphene/$SiN_{(200)}$, show the existence of amorphous carbon (Fig. 7) [32]. Our previous research shows that the SiN deposition process seems to strongly deteriorate the quality of deposited graphene [23,24].

The Raman spectra collected in the $SiN_{(300)}$/graphene/$SiN_{(200)}$ sample, showing the existence of an SiN thin film only (no evidence of carbon) (see Fig. 8). This might be caused by the fact that the $SiN_{(200)}$ layer deposited on top of the graphene layer is to thick and completely screens the Raman carbon signal from the underling graphene layer, especially if this is an amorphous carbon layer, which usually has a lower intensity than graphene [23,24].

As the obtained results show, the best structural properties were obtained for the $SiN_{(300)}$/graphene/$SiN_{(200)}$ sample with the 300 nm thick silicon nitride transition layer incorporated at the structure interface, between the titanium alloy surface and the graphene/$SiN_{(200)}$ coating system.

3.2. Potentiodynamic tests

Fig. 9a and 9b show the course of the open circuit potential (OCP) and the course of the polarization curves of all tested samples in a 0.5 M/l NaCl, 2 g/l KF, pH = 2 electrolyte solution. The results of the measurements of the electrochemical parameters of the samples obtained from the polarization curves are shown in Table 3.

The results obtained have shown that all studied SiN/graphene/SiN coating systems are highly resistant to corrosion in very aggressive environments, which is expressed by a decrease of the corrosion current

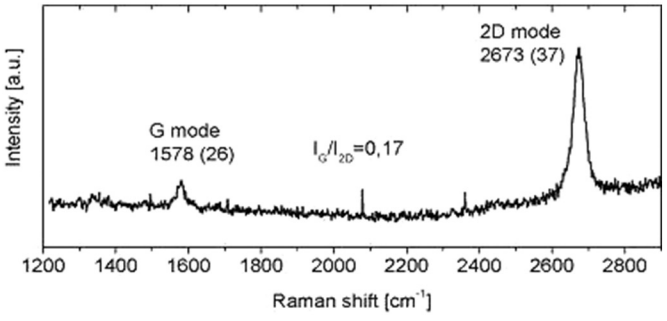

Fig. 4. An exemplary Raman spectrum of a graphene layer deposited on an SiN transition layer.

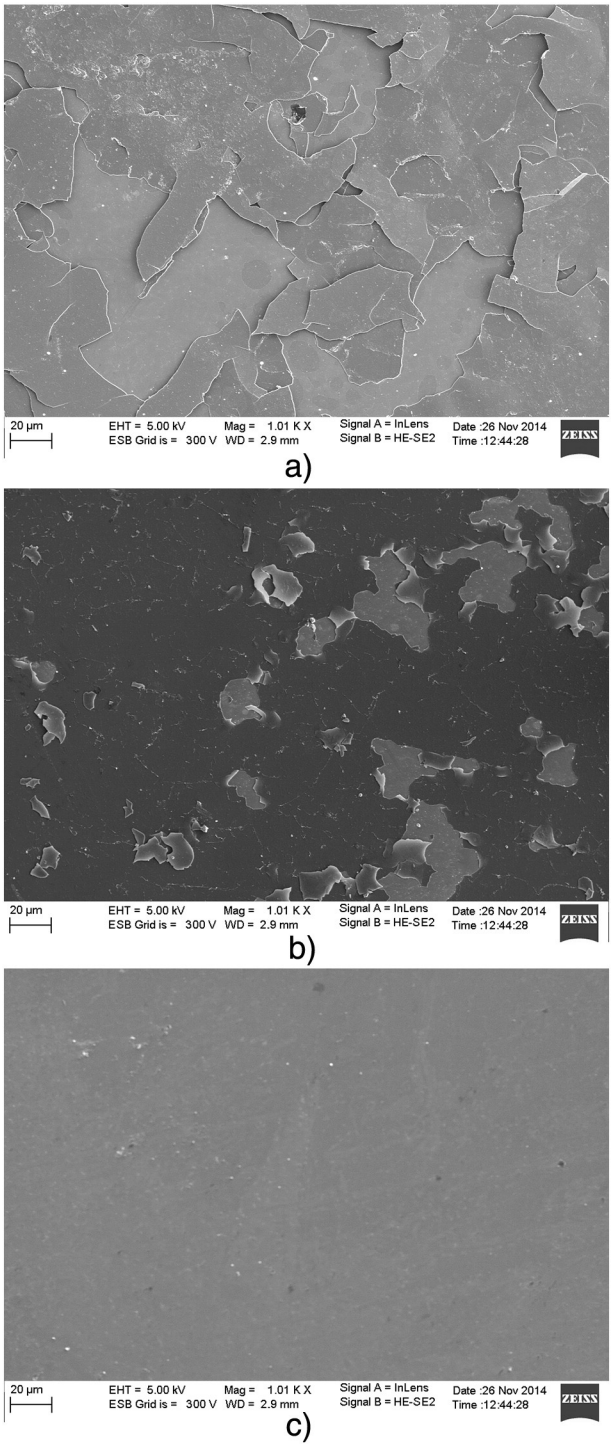

Fig. 5. SEM images of a) the $SiN_{(100)}$/graphene/$SiN_{(200)}$ coating system, b) the $SiN_{(200)}$/graphene/$SiN_{(200)}$ coating system and c) the $SiN_{(300)}$/graphene/$SiN_{(200)}$ coating system.

density i_{corr} and a shift of the corrosion potential E_{corr} values to the noble potentials.

For the samples with the $SiN_{(100)}$/graphene/$SiN_{(200)}$ and $SiN_{(200)}$/graphene/$SiN_{(200)}$ coating systems, the corrosion current density values obtained are very similar and equal $1.08 \cdot 10^{-8}$ [A/cm^2] and $2.11 \cdot 10^{-8}$ [A/cm^2], respectively. The values obtained are similar to those obtained for thicker $SiN_{(500)}$ coating systems without a graphene monolayer. This is confirmation of our previous research into the impact of graphene monolayers on the corrosion properties of thin films deposited on titanium alloy surfaces [22–24].

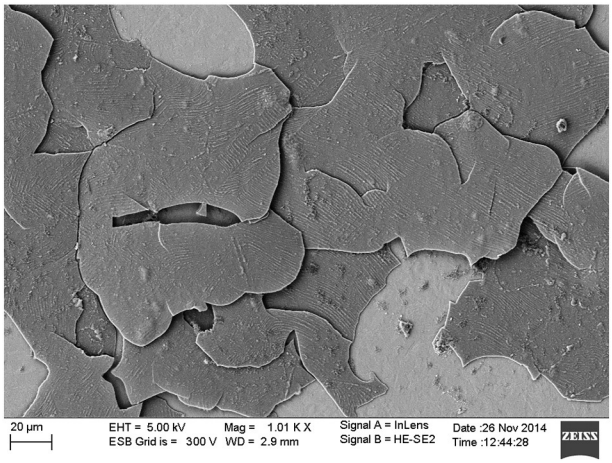

Fig. 6. An SEM image of the graphene/SiN coating system, without a transition layer.

From the all tested samples, the lowest corrosion current density and therefore the best corrosion properties were obtained for the $SiN_{(300)}$/graphene/$SiN_{(200)}$ coating system. The value of the corrosion current density obtained for the $SiN_{(300)}$/graphene/$SiN_{(200)}$ coating system was $1.11 \cdot 10^{-10}$ [A/cm^2]. This value is almost two orders of magnitude lower than the value of the corrosion current density obtained for the $SiN_{(100)}$/graphene/$SiN_{(200)}$, $SiN_{(200)}$/graphene/$SiN_{(200)}$ and $SiN_{(500)}$ coating systems.

Furthermore, the course of the voltammetric curves for titanium alloy and titanium alloy with a SiN coating (Fig. 9a) indicates the passivation of the sample surface, probably the passivation of metallic titanium. At potentials of about −0.5 V a decrease in current density occurs. This phenomenon does not occur with the other samples, i.e. titanium alloy with SiN–graphene coatings.

It should also be noted that SiN-graphene coatings have high durability, even during exposure in aggressive electrolyte. For these samples the courses of the corrosion potentials were very stable. During one hour's exposure the potential changed by only about 60 mV. For the uncoated titanium alloy sample, after about 500 s a sharp decline in the value of the potential from −0.3 V to −1.0 V takes place (see Fig. 9a). This change is caused by damage to the oxide layer present on the surface of the titanium alloy. The oxide layer acts as a barrier and protects against general corrosion processes. However, in the acidic pH (pH approx. 2) environment, the protective layer is unstable and the corrosion processes typical for metallic Ti and its alloys are initiated. This phenomenon is accelerated in the presence of aggressive ions such as

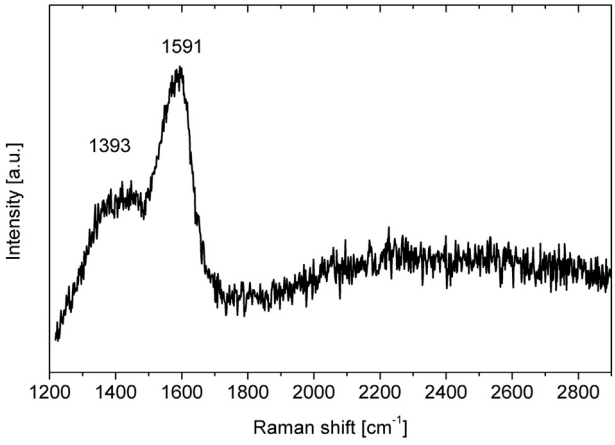

Fig. 7. Raman spectrum of a sample with the SiN layer deposited on a graphene monolayer taken in the SiN peeled-off area, showing a significantly damaged carbon layer.

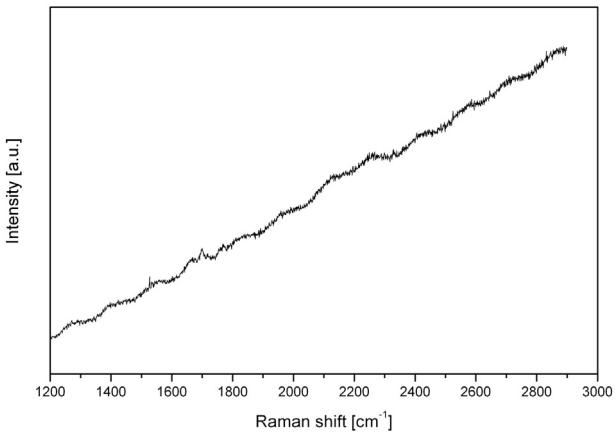

Fig. 8. Raman spectra collected in the $SiN_{(300)}$/graphene/$SiN_{(200)}$ sample.

fluoride ions [33–36]. A similar OCP course was observed for titanium alloy covered by the $SiN_{(500)}$ thin film (see Fig. 9a). In this case after about 2040s a sharp decline in the value of the potential, from −0.4 V to −0.8 V, takes place. This is probably due to the penetration of the coating by the electrolyte and the beginning of the corrosive titanium alloy reaction.

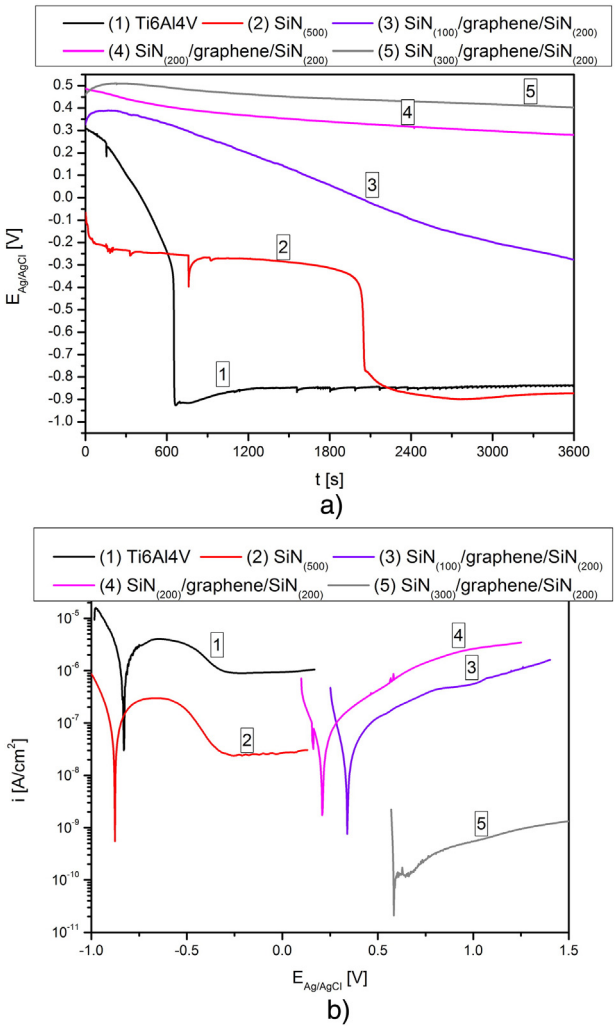

Fig. 9. Open circuit potential (OCP) (a) and polarization curves (b) of Ti6Al4V titanium alloy and titanium alloy with the $SiN_{(500)}$, $SiN_{(100)}$/graphene/$SiN_{(200)}$, $SiN_{(200)}$/graphene/$SiN_{(200)}$ and $SiN_{(300)}$/graphene/$SiN_{(200)}$ coating systems.

Table 3
Corrosion tests results of the pure titanium alloy, Ti6Al4V alloy with the $SiN_{(500)}$ coating system and Ti6Al4V alloy with the $SiN_{(100)}$/graphene/$SiN_{(200)}$, $SiN_{(200)}$/graphene/$SiN_{(200)}$ and $SiN_{(300)}$/graphene/$SiN_{(200)}$ coating systems obtained from polarization curves in a 0.5 M NaCl, pH = 2, 2 g/l KF solution.

Sample	I_{corr} [A/cm^2]	E_{corr} [V]
Ti6Al4V/$SiN_{(100)}$/gr/$SiN_{(200)}$	$1.08 \cdot 10^{-8}$	−0.49
Ti6Al4V/$SiN_{(200)}$/gr/$SiN_{(200)}$	$2.11 \cdot 10^{-8}$	−0.58
Ti6Al4V/$SiN_{(300)}$/gr/$SiN_{(200)}$	$1.11 \cdot 10^{-10}$	−0.41
Ti6Al4V/$SiN_{(500)}$	$6.72 \cdot 10^{-8}$	−0.92
Ti6Al4V	$1.25 \cdot 10^{-6}$	−0.87

The $SiN_{(300)}$/graphene/$SiN_{(200)}$ coating system is characterised by the best corrosion properties from among all the tested coating systems.

4. Summary

We have shown that a SiN transition layer incorporated at the structure interface, between the titanium alloy surface and the graphene/$SiN_{(200)}$ coating system, significantly changes its structural and corrosion properties. The structural properties of the graphene/SiN coating system depend on the thickness of the transition layer, and the thicker the transition layer, the better they are. With the 300 nm thick SiN transition layer at the structure interface, the upper silicon nitride thin film from the graphene/SiN coating system has no holes or flakes. The whole coating system is characterised by very good structural parameters and excellent corrosion resistance. Such prepared coating structure protects the titanium alloy surface against the corrosion processes that take place on pure titanium alloy surfaces in very aggressive environments.

In the next step, investigations will be performed to assess the durability of the corrosion and mechanical properties of the multilayer hybrid system (SiN/graphene) during temporary exposure in corrosive environments (artificial saliva, SBF etc.). They will involve electrochemical impedance measurements to complete the study of the corrosion properties of multilayer hybrid systems.

Acknowledgments

This work was financed by the National Centre for Research and Development in 2013–2016 as research project No. GRAF-TECH/NCBR/14/26/2013 “InGrafTi”.

References

[1] K. Elagli, M. Traisnel, H.F. Hildebrand, Electrochemical behaviour of titanium and dental alloys in artificial saliva, Electrochim. Acta 38 (1993) 1769–1774.
[2] M. Al-Mayouf, A.A. Al-Swayih, N.A. Al-Mobarak, Effect of potential on the corrosion behavior of a new titanium alloy for dental implant applications in fluoride media, Mater. Corros. 55 (2004) 88–94.
[3] R. Goldberg, J.L. Gilbert, The electrochemical and mechanical behavior of passivated and TiN/AlN-coated CoCrMo and Ti6Al4V alloys, Biomaterials 25 (5) (2004) 851–864.
[4] C.P. Dillon, Phorgotten phenomena: behavior of reactive metals, Mater. Perform. 7 (1998) 69–72.
[5] M. Nakagawa, T. Matsuya, M.O. Shiraishi, Effect of fluoride concentration and pH on corrosion behavior of titanium for dental use, J. Dent. Res. 78 (9) (1999) 1568–1572.
[6] R.W. Schutz, D.E. Thomas, Corrosion of titanium and titanium alloys, Metals Handbook, nineth ed., 13, Metals Park International American Society for Metal (ASM) 1987, p. 669.
[7] L. Kinani, A. Chtaini, Corrosion inhibition of titanium in artificial saliva containing fluoride, Leonardo J. Sci. 12 (11) (2007) 33–38.
[8] Y. Song, Z. Zhao, F. Lu, Experimental study of the influence of shot peening on the microstructure and properties of surface layer of a TC21 titanium alloy atlas, J. Mater. Sci. 1 (1) (2014) 17–21.
[9] S. Thamizhmnaii, B. Bin Omar, S. Saparudin, S. Hasan, Surface roughness investigation and hardness by burnishing on titanium alloy, J. Achievements Mater. Manuf. Eng. 28 (2) (2008) 139–142.
[10] K.-T. Rie, T. Lampe, Thermochemical surface treatment of titanium and titanium alloy Ti6Al4V by low energy nitrogen ion bombardment, Mater. Sci. Eng. 69 (2) (1985) 473–481.
[11] X. Liua, P.K. Chub, C. Dinga, Surface modification of titanium, titanium alloys, and related materials for biomedical applications, Mater. Sci. Eng. R 47 (2004) 49–121.
[12] J. Pitter, J. Cizner, F. Černý, M.A. Djouadi, A. Koutsomichalis, The influence of gradient SiNx IBAD coating on corrosion resistance of alloy steels in oxidizing and sulphidizing—oxidizing atmosphere at high temperature, Surf. Coat. Technol. 90 (1998) 1169–1173.
[13] F. Bucciotti, M. Mazzocchi, A. Bellosi, Perspectives of the Si_3N_4-TiN ceramic composite as biomaterial and manufacturing of complex-shaped implantable devices by electrical discharge machining, J. Appl. Biomater. Biomech. 8 (1) (2010) 28–32.
[14] M. Mazzocchi, A. Bellosi, On the possibility of silicon nitride as a ceramic for structural orthopedic implants. Part i: processing, microstructure, mechanical properties, cytotoxicity, J. Mater. Sci. Med. 19 (8) (2008) 2881–2887.
[15] M. Mazzocchi, D. Gardini, P. Luigi Traverso, M. Giulia Faga, A. Bellosi, On the possibility of silicon nitride as a ceramics for structural orthopaedic implants. Part II: chemical stability and wear resistance in body environment, Journal of Materials Science in Medicine 19 (8) (2008) 2889–2901.
[16] M.-C. Joa, S.-K. Park, S.-J. Park, A study on resistance of PECVD silicon nitride thin film to thermal stress-induced cracking, Appl. Surf. Sci. 140 (1999) 12–18.
[17] J. Olofsson, T. Mikael Grehk, T. Berlind, C. Persson, S. Jacobson, H. Engqvist, Evaluation of silicon nitride as a wear resistant and resorbable alternative for total hip joint replacement, Biomaterials 2 (2) (2012) 94–102.
[18] Z. Shi, Y. Wang, C. Du, N. Huang, L. Wang, C. Ning, The structure, surface topography and mechanical properties of Si–C–N films fabricated by RF and DC magnetron sputtering, Appl. Surf. Sci. 258 (4) (2011) 1328–1336.
[19] Z. Shi, Y. Wang, C. Du, N. Huang, L. Wang, C. Ning, Silicon nitride films for the protective functional coating: blood compatibility and biomechanical property study, J. Mech. Behav. Biomed. Mater. 16 (2012) 9–12.
[20] E. Teo, Y. Lih, R. Mat Zaid, T. Ling Ling, K.F. Chong, Facile corrosion protection coating from graphene, Int. J. Chem. Eng. and Appl. 3 (6) (2012) 453–455.
[21] D. Prasai, J.C. Tuberquia, R.R. Harl, G.K. Jennings, K.I. Bolotin, Graphene: corrosion-inhibiting coating, ACS Nano 6 (2012) 1102–1108.
[22] M. Kalisz, M. Grobleny, M. Mazur, D. Wojcieszak, M. Świniarski, M. Zdrojek, J. Domaradzki, D. Kaczmarek, Mechanical and electrochemical properties of Nb_2O_5, Nb_2O_5:Cu and graphene layers deposited on titanium alloy (Ti6Al4V), Surf. Coat. Technol. 271 (2015) 92–99.
[23] M. Kalisz, M. Grobelny, M. Zdrojek, M. Świniarki, J. Judek. The hybrid graphene multilayer system (graphene/SiN/graphene) coupled with titanium alloy (Ti6Al4V) — structural, mechanical and corrosion characterization. Thin Solid Films (In press) DOI: http://dx.doi.org/10.1016/j.tsf.2015.07.067.
[24] M. Kalisz, M. Grobelny, M. Zdrojek, M. Świniarki, J. Judek, Determination of structural, mechanical and corrosion properties of titanium alloy surface covered by hybrid system based on graphene monolayer and silicon nitride thin films, Thin Solid Films 583 (1) (2015) 212–220.
[25] L. Liu, W.-G. Liu, N. Cao, C.-L. Cai, Study on the performance of PECVD silicon nitride thin films, Defence Technology 9 (2013) 121–126.
[26] X. Liang, B.A. Sperling, I. Calizo, G. Cheng, C.A. Hacker, Q. Zhang, Y. Obeng, K. Yan, H. Peng, Q. Li, X. Zhu, H. Yuan, A.R. Hight Walker, Z. Liu, L. Peng, C.A. Richter, Toward clean and crackless transfer of graphene, ACS Nano 5 (2011) 9144–9153.
[27] A. Jorio, R. Saito, G. Dresselhaus, M.S. Dresselhaus, Raman Spectroscopy in Graphene-Based Systems: Prototypes for Nanoscience and Nanometrology, Wiley-VCH, 2011.
[28] V. Singh, D. Joung, L. Zhai, S. Das, S.I. Khondaker, S. Seal, Graphene based materials: past, present and future, Prog. Mater. Sci. 56 (2011) 1178–1271.
[29] A. Gupta, G. Chen, P. Joshi, S. Tadigadapa, P.C. Eklund, Raman scattering from high-frequency phonons in supported n-graphene layer films, Nano Lett. 6 (2006) 2667–2673.
[30] A.C. Ferrari, J.C. Meyer, V. Scardaci, C. Casiraghi, M. Lazzeri, F. Mauri, S. Piscanec, D. Jiang, K.S. Novoselov, S. Roth, A.K. Geim, Raman spectrum of graphene and graphene layers, Phys. Rev. Lett. 97 (2006) 187401.
[31] F. Mansfeld, Electrochemical methods of corrosion testing, ASM International ASM Handbook 13A (2003) 446–462.
[32] P.K. Chu, L. Li, Characterization of amorphous and nanocrystalline carbon films, Mater. Chem. Phys. 96 (2006) 253–277.
[33] G. Boere, Influence of fluoride on titanium in an acidic environment measured by polarization resistance technique, J. Appl. Biomater. 6 (4) (1995) 283–288.
[34] M. Nakagawa, S. Matsuya, T. Shiraishi, M. Ohta, Effect of fluoride concentration and pH on corrosion behavior of titanium for dental use, J. Dent. Res. 78 (1999) 1568–1572.
[35] R.W. Schutz, D.E. Thomas, Corrosion of titanium and titanium alloys, Metals Handbook, 13, American Society for Metal (ASM) International, Metals Park, OH 1987, pp. 669–706.
[36] L. Kinani, A. Chtaini, Corrosion inhibition of titanium in artificial saliva containing fluoride, Leonardo J. Sci. 6 (11) (2007) 33–40.